SUPPORTING INFORMATION

Automated 4-Sample Protein Immunoassays using 3D-Printed Microfluidics

Karteek Kadimisetty,[a] Andrew P. Spak,[a] Ketki S. Bhalerao,[a] Mohamed Sharafeldin,[a,b] Islam M. Mosa,[a,c] Norman H. Lee[d] and James F. Rusling[*,a,e,f]

[a]Department of Chemistry and Institute of Material Science, University of Connecticut, Storrs, Connecticut 06269, United States
[b]Department of Analytical Chemistry, Faculty of Pharmacy, Zagazig University, Zagazig, Egypt
[c]Department of Chemistry, Tanta University, Tanta 31527, Egypt
[d]Department of Pharmacology & Physiology, George Washington University, Washington, D.C. 20037, United States
[e]Department of Surgery and Neag Cancer Center, UConn Health, Farmington, Connecticut 06032, United States
[f] School of Chemistry, National University of Ireland, Galway H91 TK33, Ireland

Table of Contents.

Additional experimental details

3D Printing. The immunoarray was 3D printed on a Form 1+ SLA printer from Formlabs (Somerville, MA). Initially a computer aided design (CAD) with required features were generated using 123D design software (Autodesk), Fig. 2 and later converted to 3D printer compatible file using splicing software preform. The preform file with 3D design was subjected to selected optimized orientation and generated supports to produce final print file. The print orientation was adjusted onto the build platform so that the reagent chambers in the array are longitudinal while printing, this allowed the channels to flush the resin automatically through the vent holes. The layer height was selected to be 50 μm that gave us faster prints without sacrificing the print quality and resolution. The printed arrays were then removed from the build platform, supports were removed, submerged into isopropanol and subjected to sonication for 15 min to remove any uncured resin present on the outside or inside of the array. The dried arrays were then spray coated with clear acrylic spray (Krylon™) and allowed to air dry for an hour to adjust the transparency to clear for ECL detection.

The reagents/sample were added through a 0.8 mm hole present at the top of the reagent chamber. We call them injection ports and we also assembled few more ports called vent holes between each turns to facilitate reproducible filling of the chambers, Fig. 2A & B. The holes on the both ends of the chambers in the turns helps to fill the chambers evenly without choosing a direction. As we are dealing with tiny volume in a confined space, the added reagents will replace the air in the chamber. These vent holes near the ends of each chamber pushes the air out of the chambers as the liquids enter the chamber resulting in precise addition of reagents. This is rather an important part of our design and we optimized the position of these vent holes for precision of reagent/sample loading. This also ensured better control over automated reagent delivery to detection chamber. We used calibrated micropipettes to add the reagents/samples into

their respective chambers prior to immunoassay. The detection chamber was equipped with holes and grooves to hold 0.4 mm platinum counter electrode wire and 0.6 mm Ag/AgCl reference electrode wire that run parallel within the detection chamber to complete a 3 electrode setup with pyrolytic graphite sheets as working electrodes.

Besides PGS electrodes being flexible, ultrathin and highly conductive that aids in overall miniaturization, they are also highly stable towards harsh organic solvents like dimethylformamide (DMF). Most of the commercial screen printed electrodes are unstable in organic solvents to show a comparison we performed an electrochemical study that highlights the stability of PGS electrodes used in this study, Fig. S2, SI. We incubated PGS electrodes along with two other commercially available screen electrodes in 100% DMF for 10 min at room temperature and further observed change in electrochemically active surface area. Besides the selection of DMF is apt for this study as the SWCNTs that are used to build SWCNT forest on PGS are dispersed in DMF. The results suggested minimal electrochemical surface area change from 7.88×10^{-3} (before treatment) to 8.12×10^{-3} for PGS electrodes with standard deviation $\leq$ 10% whereas for Kanichi® screen printed carbon electrodes the electrochemical surface area changed from 7.13×10^{-4} to 3.51×10^{-4} with standard deviation > 25% and for pine research® screen printed electrodes there is significant change from 2.11×10^{-3} to 1.83×10^{-1} due to loss of insulation layer under influence of DMF Table S1, Fig. S3, SI.

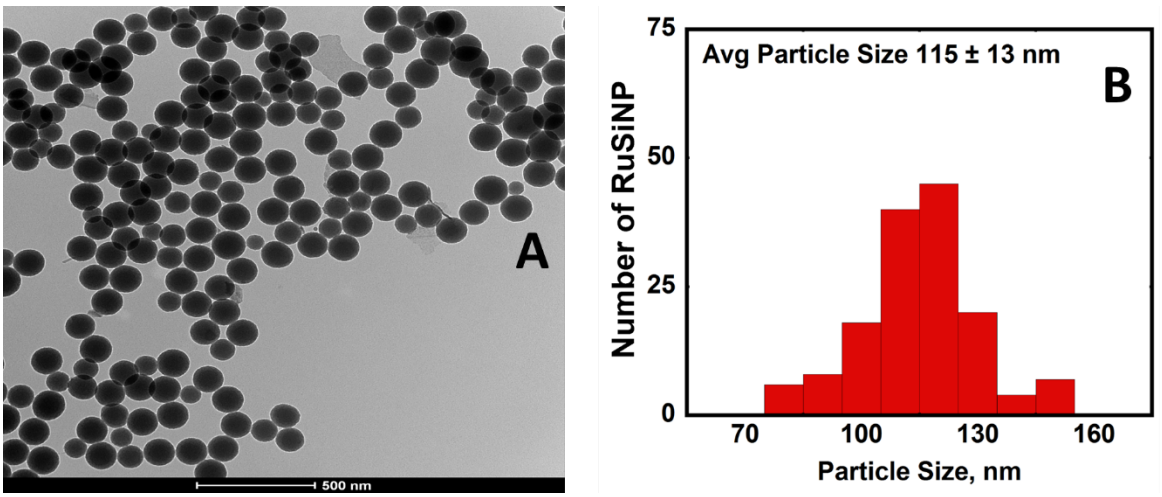

Fig. S1 (A) TEM image of RuBPY-silica nanoparticles on a 500 nm scale bar. (B) Size distribution of RuBPY silica nanoparticles with an average diameter of 115 ± 13 nm.

Effect of DMF on the screen-printed carbon electrodes and PGS sheets

The effect of dimethylformamide (DMF, used to assemble SWCNT forests on detection chips) on the performance of commercially available screen-printed electrodes and PGS sheets was evaluated. The surface area of each electrode was estimated before and after exposing the electrode surface to 500 µL of DMF for 10 minutes. Kanichi® electrodes and Pine Research® electrodes were used as samples of screen-printed electrodes and compared to electrodes made with Panasonic® PGS. Electrochemical active surface area of each electrode was estimated, using Randle-Sevcik equation. Calculations were based on the slope of cyclic voltammogram peak currents of 5 µM potassium ferricyanide ($K_3Fe(CN)_6$) in in 1.0 M potassium chloride (KCl) against the square root of the scan rate ($v^{1/2}$). Fig. 1 shows plots of each electrode before and after exposure to DMF. Calculated slope according to Randle-Sevcik equation is equal to ($2.69 \times 10^5 n^{3/2} A D^{1/2} C$) [where, n: electron stoichiometry, A: electrochemical surface area, D: diffusion

coefficient of $K_3Fe(CN)_6$ in KCl = 6.5 X 10^{-6} cm^2/s, and C: molar concentration of $K_3Fe(CN)_6$.

Table S1 indicate the surface area of each electrode before and after treatment with DMF.

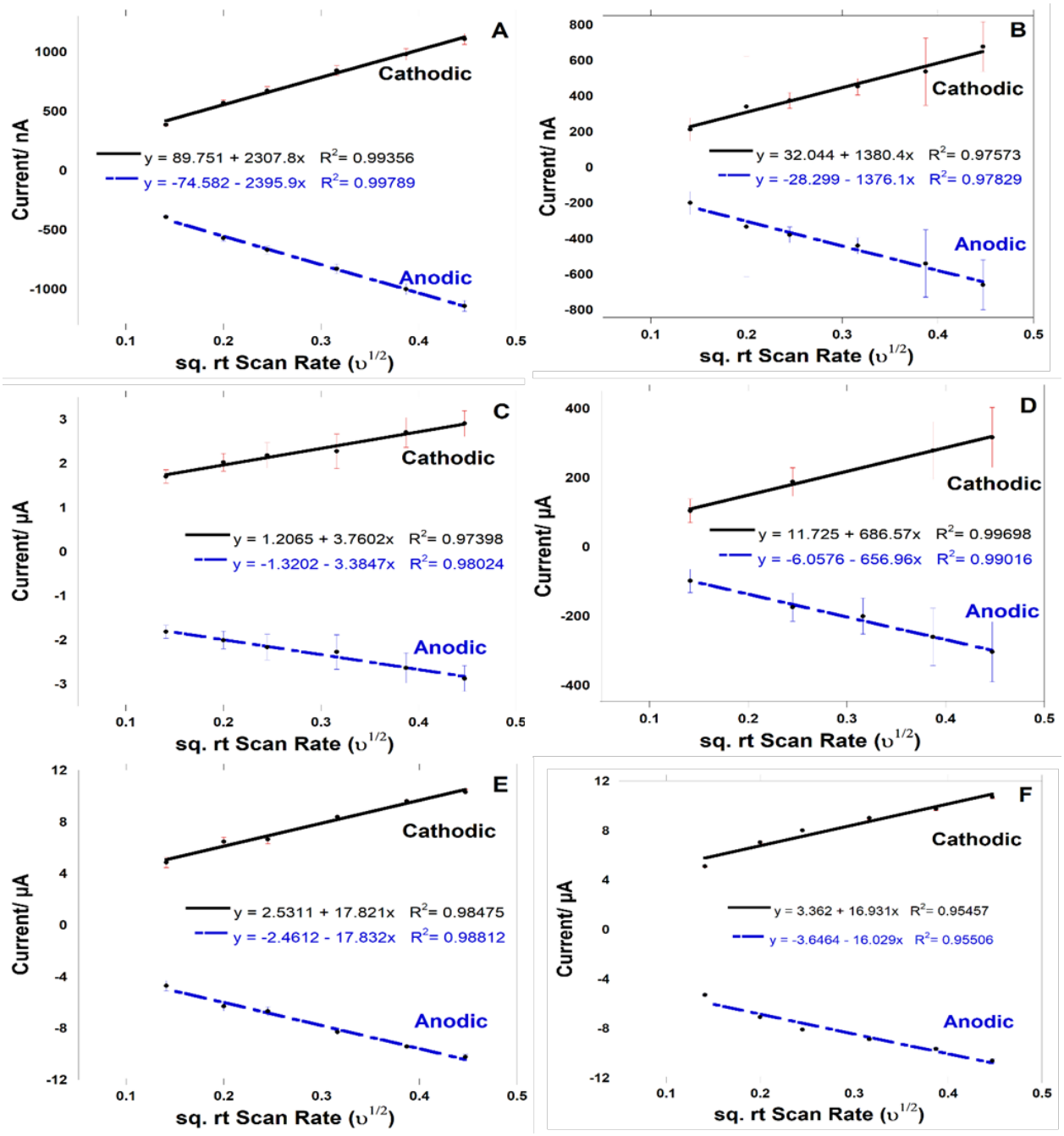

Fig. S2. Plots of peak current vs. square root of the scan rate for the Kanichi® electrodes before (A) and after (B) DMF exposure, Pine Research® electrodes before (C) and after (D) DMF exposure and Graphene sheets before (E) and after (F) DMF treatment. Measurements were done

by running cyclic voltammograms for each electrode at different scan rates in 5.0 µM $K_3Fe(CN)_6$ in 1.0 M KCl Vs Standard Calomel electrode and platinum counter electrode.

DMF treatment resulted in a decrease of the electrochemical active surface area of Kanichi® electrodes suggesting solubilization of the carbon ink and also suggested by the increased standard deviation of the electrode surface area after DMF exposure. For Pine Research electrodes®, DMF could be visually seen to dissolve the insulator layer (Fig. 2) exposing electrodes and electrodes connections thus increasing surface area and standard deviations. In case of PGS sheets, we did not find any visual deformation or statistically significant changes in surface area before and after DMF exposure.

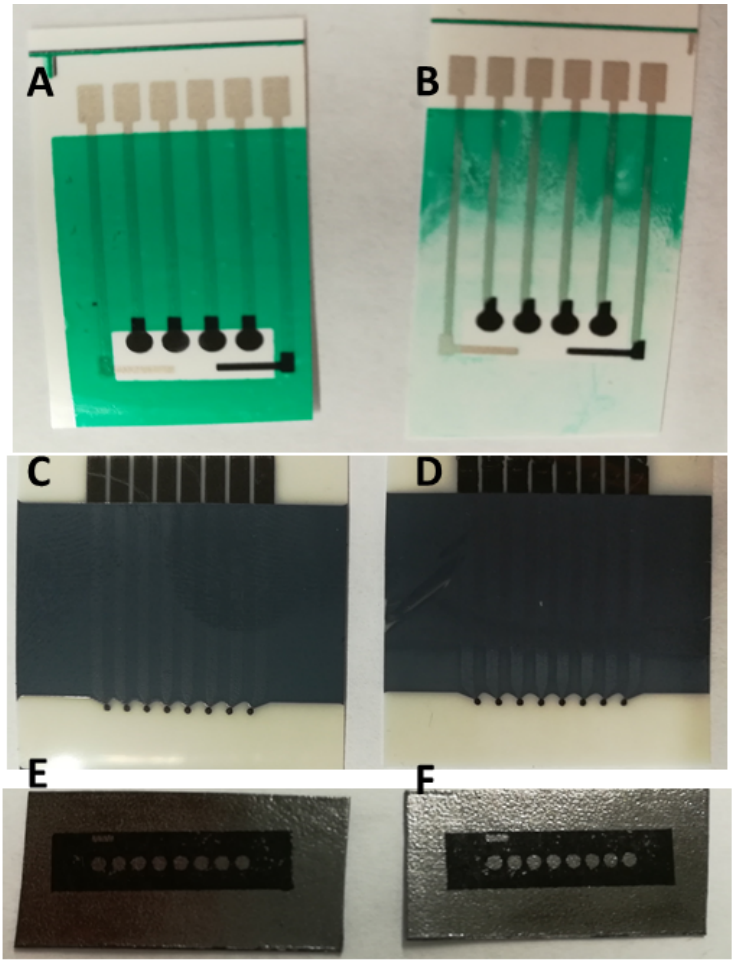

Fig. S3 Pictures of Pine Research® electrodes before (A) and after (D) DMF exposure, Kanichi® electrodes before (C) and after (D) DMF exposure, and Graphene sheets before (E) and after (F) DMF treatment.

Table S1: Electrode surface area indicating the change after exposure to DMF

Electrode	Before DMF treatment			After DMF treatment		
	Average Surface Area (cm^2)	Standard Deviation	% Standard Deviation	Average Surface Area (cm^2)	Standard Deviation	% Standard Deviation
Kanichi®	7.13×10^{-4}	5.95×10^{-5}	± 8%	3.51×10^{-4}	9.22×10^{-5}	± 26%
Pine Research®	2.11×10^{-3}	2.42×10^{-4}	± 11%	1.83×10^{-1}	7.35×10^{-2}	± 40%
Panasonic® PGS	7.88×10^{-3}	8.73×10^{-4}	± 11%	8.12×10^{-3}	8.37×10^{-4}	± 10%

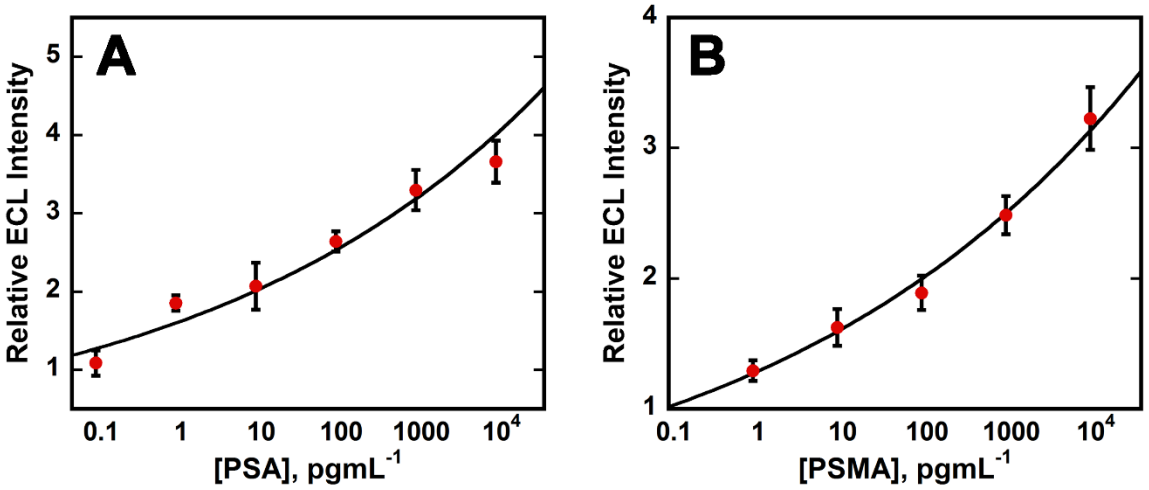

Fig. S4 Calibration curves in undiluted calf serum with ECL responses captured over 180 s, (A) PSA and (B) PSMA vs concentration with applied ECL generation potential of 1V vs. Ag/AgCl. Error bars show standard deviation, n=4.

Table S2. Concentration of PSA and PSMA obtained from multiplexed ECL immunoassay for both prostate cancer and prostate cancer negative patient samples.

PS #	ECL PSA ng/mL	ECL PSMA ng/mL
1	7.2	803.7
2	2.4	433.0
3	4.9	227.7
4	4.4	865.7
5	4.4	1475.6
6	2.9	24.3
7	11.6	732.1
8	2.1	313.2
9	8.2	386.2
10	1.1	378.4
11	3.7	363.1
12	7.6	427.3
13	3.0	194.7
14	1.1	173.9
15	4.5	142.3
16	6.3	345.8
17	2.8	84.0
18	4.1	526.2
19	4.9	477.8
20	4.8	152.3
21	6.3	308.8
22	3.2	30.4
23	6.5	560.4
24	5.7	274.9
25	5.2	289.3
26	1.5	50.9
27	6.1	596.4
28	5.4	61.6
29	6.5	54.3
30	3.5	143.5
31	0.4	20.2
32	2.3	66.2
Neg_1	2.7	86.6
Neg_2	1.1	38.9
Neg_3	1.6	19.6
Neg_4	1.7	64.5
Neg_5	2.0	42.1
Neg_6	0.2	13.5

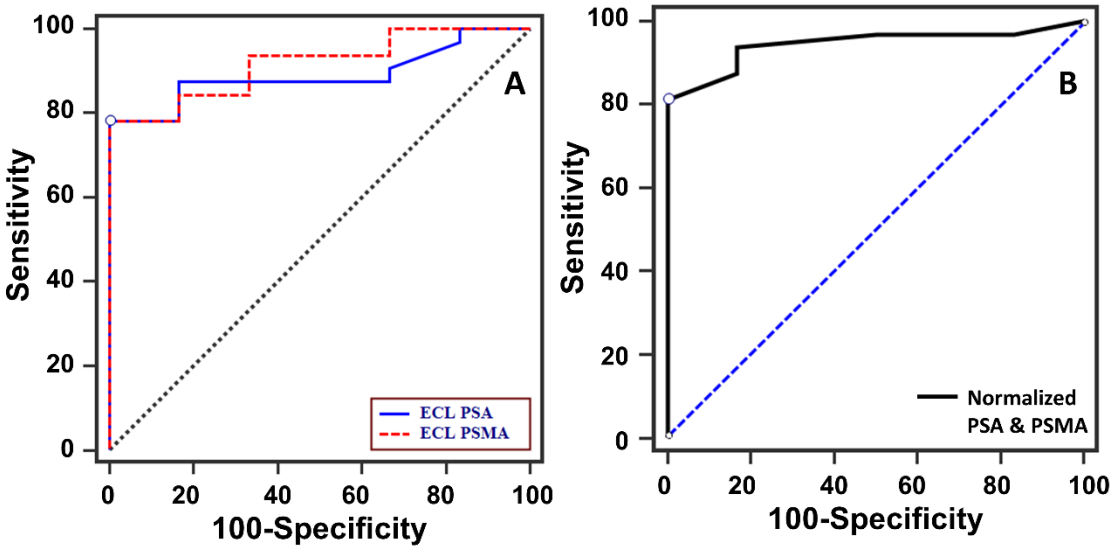

Fig. S5 Receiver operating characteristic curves (ROC) for 38 human serum samples. (A) Red line for PSMA and Blue line for PSA shows AUC to be 0.89 for PSA, 100 % specificity and 78.1 % sensitivity and for PSMA, AUC was calculated to be 0.92, 100 % specificity and 78.1 % sensitivity. (B) Normalized PSA and PSMA results suggest 0.95 AUC, 100 % specificity and 81.3 % sensitivity.

.